An evaluation of the effects of SiC layer thinning on failure of TRISO-coated fuel particles

Gregory K. Miller *, David A. Petti, John T. Maki, Darrell L. Knudson

Idaho National Laboratory, P.O. Box 1625, Idaho Falls, ID 83415-3855, USA

Abstract

The fundamental design for a gas-cooled reactor relies on the behavior of the coated particle fuel. The coating layers surrounding the fuel kernels in these spherical particles, consisting of pyrolytic carbon and silicon carbide layers, act as a pressure vessel that retains fission products. Many more fuel particles have failed in US irradiations than would be expected when only one-dimensional pressure vessel failures are considered. Several multi-dimensional failure mechanisms that may have contributed to these failures have been previously studied, such as (1) irradiation-induced shrinkage cracks in the inner pyrocarbon (IPyC) layer, (2) partial debonding between the IPyC and SiC layers, and (3) deviations from a perfectly spherical shape. A further phenomenon that could lead to particle failures is thinning of the SiC layer caused by either thermal decomposition or interaction with fission products. Results of a study of the effects of SiC thinning and criteria for evaluating this behavior in a fuel performance code are presented.
© 2006 Elsevier B.V. All rights reserved.

1. Introduction

The success of gas-cooled reactors depends largely upon the safety and quality of the coated particle fuel. The coating layers of a particle, which surround the fuel kernel and buffer, consist of an inner pyrolytic carbon (IPyC) layer, a silicon carbide (SiC) layer, and an outer pyrocarbon (OPyC) layer. These layers act as a pressure vessel for fission product gases as well as a barrier to the migration of other fission products. The quality of the fuel can be characterized by the number of particle failures that occur during reactor operation. A performance model of the coating layers, which predicts the failure probability for a population of fuel particles, must account for all viable mechanisms that can lead to particle failure.

Aside from the traditional pressure vessel failure mechanism, several mechanisms involving multi-dimensional behavior of fuel particles may contribute to particle failures. These include the presence of radial shrinkage cracks in the IPyC layer, partial debonding between the IPyC and OPyC layers, and deviations from a spherical shape. To aid in investigating the effects of these various forms of multi-dimensional behavior, we are developing an integrated mechanistic fuel performance modeling code called PARticle FUel ModEl (PARFUME).

* Corresponding author. Tel.: +1 208 526 0360; fax: +1 208 526 2930.
  E-mail address: GregoryK.Miller@inl.gov (G.K. Miller).

The methodology for incorporating these failure mechanisms into the performance model has been developed [1,2]. An additional phenomenon that could potentially lead to the failure of TRISO-coated particles is thinning of the SiC layer. This is caused by either thermal decomposition or interaction with fission products, associated mainly with accident conditions at high temperatures. Thinning is expected to occur in local regions when caused by SiC interaction with certain fission products such as palladium. It is expected to occur more globally (i.e., over large portions of the SiC surface area) when caused by interaction with CO or by SiC thermal decomposition at high temperatures. Failure evaluations have been performed for various scenarios of SiC thinning to determine the effects of (1) local vs. global thinning, (2) the size of thinned regions (width and depth), (3) the number of locations at which thinning occurs, (4) sharp corners vs. smooth transitions at the edges of thinned regions and (5) stresses caused by shrinkage of the pyrocarbon layers and by internal pressure loading on failure due to SiC thinning. Results of these evaluations are used to form the basis for failure criteria for SiC thinning to be implemented in PARFUME.

2. Behavior of the coating layers

The basic behavior of the three coating layers of the TRISO-coated particle is shown in Fig. 1. Fission gas pressure builds up in the kernel and buffer regions, while the IPyC, SiC, and OPyC act as structural layers to retain this pressure. The IPyC and OPyC layers both shrink and creep during irradiation of the particle while the SiC exhibits only elastic response. A portion of the gas pressure is transmitted through the IPyC layer to the SiC. This pressure generally increases as irradiation of the particle progresses, thereby contributing to a tensile hoo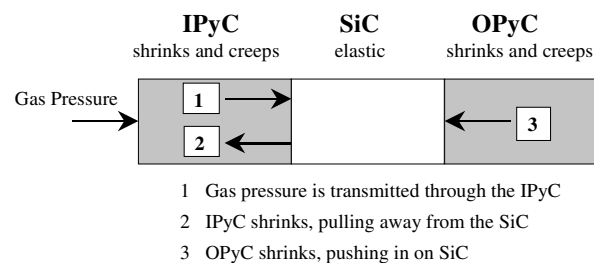p stress in the SiC layer. Countering the effect of the pressure load is the shrinkage of the IPyC and OPyC layers during irradiation, which causes them to push or pull inward on the SiC. Due to anisotropy in the pyrocarbon shrinkage behavior, the shrinkage histories differ in the radial and tangential directions. The shrinkage in the radial direction reverses to swelling at moderate fluence levels, whereas shrinkage in the tangential direction continues to high fluence levels.

In the stress analyses performed for this evaluation, an internal pressure is applied to the IPyC to simulate the fission gas build-up. The shrinkage strain rates and creep coefficients for the pyrocarbons and the elastic properties for the pyrocarbons and the SiC were obtained from data that was compiled in a report by General Atomics in 1993 [3]. As such, the shrinkage strains are treated as functions of the following four variables: fast neutron fluence, pyrocarbon density, degree of anisotropy [as measured by the Bacon Anisotropy Factor (BAF)], and irradiation temperature. Irradiation-induced creep is treated as secondary creep, with a coefficient that is a function of pyrocarbon density and irradiation temperature. The creep coefficients used in our analyses were set equal to twice the values recommended in the General Atomics data. This is closer to what is used in older performance models [4,5], and has resulted in predictions that are in better agreement with results from irradiation experiments of the New Production – Modular High Temperature Gas Cooled Reactor Program [6]. The elastic modulus for the pyrocarbon layers is applied as a function of four variables (the same variables as used for shrinkage), while the elastic modulus for the SiC is applied as a function of temperature only.

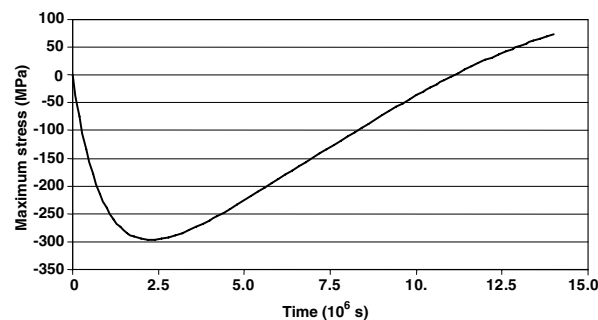Fig. 2 plots a time evolution for the tangential stress at the inner surface of the SiC layer for a

Fig. 1. Behavior of coating layers in a fuel particle.

1 Gas pressure is transmitted through the IPyC
2 IPyC shrinks, pulling away from the SiC
3 OPyC shrinks, pushing in on SiC

Fig. 2. Tangential SiC stress history for a normal particle.

normal spherical particle that is irradiated to a fluence level of 3.5×10^{25} n/m^2 (occurring at a time of 1.4×10^7 s in the analysis). Early during irradiation, the shrinkage of the pyrocarbon layers induces an increasing compressive stress in the SiC. Eventually, creep in the pyrocarbon layers relieves stress in those layers, diminishing the beneficial effect of the shrinkage. Therefore, the tangential stress in the SiC reaches a minimum value, then steadily increases through the remainder of irradiation. A traditional pressure vessel failure is expected to occur if the tangential stress reaches a tensile value that exceeds the strength of the SiC for that particle.

3. Local thinning

3.1. Model and input parameters

Attack of the SiC layer by fission products such as palladium occurs in local areas, and was the first type of thinning evaluated in this study. A three-dimensional finite element model of a TRISO-coated particle as shown in Fig. 3 was required to make this evaluation. The thinning was modeled by removing elements from the model in the thinned region of the SiC layer. Stresses caused by the thinning are determined by performing a 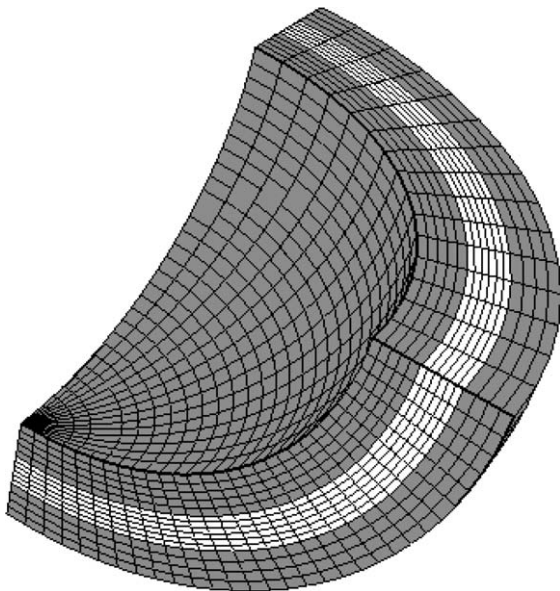finite element stress analysis using the ABAQUS computer program [7]. These stresses are then used to calculate a failure probability due to the SiC thinning, recognizing that the SiC strength varies among particles according to a Weibull statistical distribution. The probabilities reported here reflect only this statistical variation in SiC strength. Thus, the failure probabilities lose some accuracy because they do not include the effects of other statistical variations that occur, such as in the thicknesses of the coating layers and the kernel diameter. While the probability determined for a specific particle batch is not intended to be precise, changes in probability associated with changes in the thinning scenario are indicative of trends that can be expected. When the SiC thinning mechanism is modeled in the PARFUME code, statistical variations in important input parameters will be treated with the same statistical methodology as is used for other multi-dimensional phenomena [2,6].

Values used for important parameters in the analyses are summarized in Table 1. The particle analyzed has the dimensions of a standard particle for the Department of Energy Advanced Gas Reactor program.

It is noted that the depth of the thinned region was assumed to reach the full thickness of the SiC layer. This was done to conservatively determine the effect of local thinning on the structural behavior of the particle. Thinning through the entire thickness of the SiC layer will be considered a particle failure in the performance model, since this

Fig. 3. ABAQUS three-dimensional finite element model of TRISO-coated fuel particle used for evaluating local thinning of the SiC layer.

Table 1
Parameters assumed in the analyses

Quantity	Units	Value
Temperature	K	1273
Internal pressure	MPa	30
Kernel diameter	μm	350
Buffer thickness	μm	100
IPyC thickness	μm	40
SiC thickness	μm	35
OPyC thickness	μm	40
PyC density	Mg/m^3	1.90
PyC BAF		1.02
End-of-life fluence	n/m^2, $E > 0.18$ MeV	4×10^{25}
Size of thinned region, width × width	μm	17 × 29
Depth of thinned region	μm	35 (full SiC thickness)
Weibull characteristic strength, SiC [3]	MPa-μm$^{3/6}$	9640
Weibull modulus, SiC [3]		6

provides an open path for fission product transport. These functional failures, however, are not included in the failure probabilities presented here.

3.2. Failure evaluation

The model shown in Fig. 3 constitutes one-eighth of the entire spherical particle. Symmetry boundary conditions are applied to the three faces at the edges of the model to simulate a full sphere. As such, the presence of one thinned region in the one-eighth model simulates eight thinned regions over the entire sphere. Thinning of the SiC can affect particle behavior in two basic ways. First, shrinkage of the pyrocarbons induces stress concentrations in the SiC around the edges of the thinned regions. Tensile stress components in the areas of stress concentration can enhance the probability that the SiC fails. Failures associated with pyrocarbon shrinkage are likely to occur relatively early during irradiation when shrinkage effects are greatest. Second, thinning of the SiC could result in increased stresses due to internal pressure. Failures associated with the internal pressure are likely to occur later during irradiation, when the internal pressure loading is most significant. In the calculations performed, failure probabilities, P_f, for the SiC layer were determined according to the Weibull statistical theory from the characteristic strength σ_0 and modulus m as follows [8]:

$$P_f = 1 - e^{-\int_V (\sigma/\sigma_0)^m dV}, \tag{1}$$

where V is the volume of the SiC layer.

Once finite element results were obtained from the ABAQUS analysis of a thinned particle, the stress integration over the volume of the SiC layer was performed using the principle of independent action model for treating multiaxial stress states [8]:

$$\int_V \sigma^m dV = \int_V (\sigma_1^m + \sigma_2^m + \sigma_3^m) dV, \tag{2}$$

where σ_1, σ_2, and σ_3 are principal stress components in three orthogonal directions. Since only tensile stresses contribute to fracture of the material, compressive stresses were not included in the integration. The integration was performed using stress values calculated at integration points in the ABAQUS analysis.

The uncertainty in data currently available for the SiC Weibull strength parameters (σ_0 and m) and other material properties will affect the calcu-

lated failure probabilities. For a typical case, an error of 10% in the SiC characteristic strength σ_0 would affect the calculated failure probability by nearly a factor of 2, while an error of 10% in the modulus m would affect the probability by about an order of magnitude. It is also noted that the Weibull parameters used in the study may not truly represent the fracture behavior of the coating layers in a corroded condition. A crack propagation model based on fracture properties of the corroded material could show that the material is more sensitive to failure than realized in these analyses.

Calculated failure probabilities due to stresses caused by shrinkage of the pyrocarbon layers for two scenarios are summarized in Table 2. In the first case, a single thinned region is contained in the one-eighth finite element model, simulating eight thinned regions over a full sphere. In the second case, five thinned areas are spaced at uniform intervals over the one-eighth model, simulating 40 attack areas over a full sphere. The results show that localized thinning of the SiC makes a negligible contribution to failure of the particles, even if a large number of thinned areas are considered. Table 2 also shows the percentage of the total SiC surface area that is thinned in the two cases. In the case of 40 attack zones, the zone areas vary somewhat because of variations in the size of the finite elements from one thinned location to another.

A second set of calculations were performed where the internal pressure was increased from 30 to 100 MPa, to determine the effect of the presence of locally thinned areas on the failure probability associated with very high internal pressure loading. A large pressure was applied to bring the reference failure probability (with no thinned regions) to a significant level. The results, summarized in Table 3, show that the presence of the thinned locations only mildly increases the failure probability from that of a condition of no thinned locations. The second case in Table 3 (one thinned location) was made

Table 2
Failure probability vs. number of thinned locations, internal pressure = 30 MPa

Number of through-wall thinned locations	Percentage of total surface area removed	Failure probability
8	0.29	1.46×10^{-8}
40	1.32	2.68×10^{-8}

Table 3
Failure probability vs. number of thinned locations, internal pressure = 100 MPa

Number of through-wall thinned locations	Percentage of total surface area removed	Failure probability
0	0	0.1687
1	0.036	0.1714
8	0.29	0.1762
40	1.32	0.2060

Table 4
Effect of asphericity on failure probability, no thinned regions, internal pressure = 100 MPa

Aspect ratio	Failure probability
1.0	0.1687
1.027	0.2773

possible with the one-eighth model by including only effects of stress concentrations in one thinned region in the volume integration of Eq. (2). It is noted that these cases are hypothetical illustrations only, and are not intended to characterize actual particles.

Table 4 shows the effect on failure probability due to the internal pressure of 100 MPa when a moderate amount of asphericity is introduced (with no thinned regions). The asphericity was represented with a flat facet and an aspect ratio (ratio between major and minor outside diameters for the particle) of 1.027, which is representative of what can be expected in a typical particle. As shown, the asphericity (Table 4) increased the failure probability much more significantly than did the presence of thinned regions (Table 3). Thus, the effect of even a moderate amount of asphericity largely overwhelms the effect of local SiC thinning when internal pressure loading is applied.

The results of the evaluations on local thinned regions indicate that this type of thinning does not make a meaningful contribution to the failure probability at the pressure expected in a particle under normal operation (<30 MPa), and only a minor contribution at high pressures (relative to asphericity effects). Because thinning through the entire SiC thickness does constitute a functional failure of a particle, since it opens a path for fission product transport, the recommended failure criterion for local thinning is that failure occurs when penetration through the full SiC thickness is achieved.

4. Global thinning, analyzed with axisymmetric model

Axisymmetric models, such as those shown in Table 5, were utilized to evaluate several of the effects of global thinning of the SiC layer. These axisymmetric models provided a convenient means for assessing the effect that the following factors have on the particle failure probability: (1) depth and width of the attack zone, (2) sharp corners vs. a smooth transition at the edges of the zone, and (3) the number of locations at which thinning occurs. The thinning considered in these models is labeled 'global' because the thinned region extends over the full circumference of the particle rather than just a local area. Failure probabilities were again calculated using the Weibull statistical theory as given by Eq. (1). Analyses were performed using the input parameters shown in Table 1.

4.1. Sharp corner at transition between thinned and nonthinned regions

The thirteen models of Table 5 simulate thinned regions of various shapes to evaluate the effect that the depth, width, and the number of thinned areas have on the failure probability. Though the thinned regions in these models extend around the circumference of the SiC layer, the thinned areas are still generally limited to a small fraction of the full SiC surface area. The failures that occur with these partially thinned models are caused by shrinkage of the pyrocarbon layers, which induces stress concentrations at the edges of the thinned regions. (When thinning occurs over a large portion of the SiC surface area, internal pressure loading can also significantly contribute to particle failures. This type of thinning is addressed in Section 5.) Sharp corners exist at the transition between thinned and nonthinned regions for the models in Table 5, except for Case 2. These notches are expected to be representative of cases where thinning occurs over narrow regions. (Models having a smooth transition at the edges of the thinned regions are discussed in Section 4.2.) The results of Table 5 show that the failure probability increases with either an increased depth or an increased width of the thinned region, but is more sensitive to an increased width. They also show that the failure probability remains relatively moderate even at large penetration depths. Cases 12 and 13 address the effect of increasing the

Table 5
Calculated failure probabilities for several configurations of a thinned SiC layer
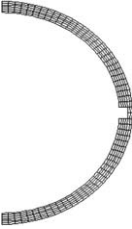
Model	Case number, description	Size, depth × width (µm)	Failure probability
	1 thinned through 1/6 of SiC wall thickness	5.8×104	6.28×10^{-5}
	2 same as Case 1, except transition at edge of thinned area is smoothed ('tenth' model)	5.8×104	5.11×10^{-6}
	3 depth increased by factor of 2 relative to Case 1	11.7×104	1.05×10^{-4}
	4 width increased by factor of 2.7 relative to Case 1	5.8×279	5.71×10^{-4}
	5 narrow zone of thinning	11.7×52.2	2.91×10^{-6}
	6 depth is increased relative to Case 5	17.5×52.2	6.92×10^{-6}

Table 5 (*continued*)
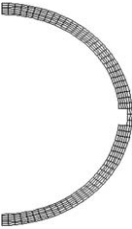
Model	Case number, description	Size, depth × width (µm)	Failure probability
	7 depth is increased relative to Case 6	23.3 × 52.2	2.47×10^{-5}
	8 depth is increased relative to Case 7	29.2 × 52.2	1.71×10^{-4}
	9 very narrow, deep penetration	23.3 × 17.4	3.24×10^{-6}
	10 width is increased relative to Case 9	23.3 × 34.8	9.17×10^{-6}
	11 width is increased relative to Case 10	23.3 × 69.6	6.03×10^{-5}
	12 Case 10 zone size applied at two locations	23.3 × 34.8 each location	1.60×10^{-5}

Table 5 (*continued*)

Model	Case number, description	Size, depth × width (µm)	Failure probability
	13 Case 10 zone size applied at five locations	23.3 × 34.8 each location	3.37×10^{-5}

number of thinned locations to two and five, respectively. Results showed that the failure probability increased by factors of 1.7 and 3.7, respectively, for these cases.

4.2. Smooth transition between thinned and nonthinned regions

Smooth transitions between the thinned and nonthinned regions were also considered. This type of transition is expected to be more representative of situations where thinning occurs over broader areas of the SiC surface. Because a smooth transition reduces the stress concentrations associated with the discontinuity at the edges of the thinned region, the resulting failure probabilities are expected to be lower. The model in Case 2 of Table 5 is identical to that of Case 1 except that it has a smooth transition, which resulted in about an order of magnitude reduction in the failure probability. This model is referred to as the 'tenth' model because thinning occurs over one-tenth of the SiC surface area.

Fig. 4 illustrates smooth transitions for three stages of penetration affecting one-half of the SiC surface area. Similar analyses were performed on particles where one-quarter and one-tenth of the surface area were thinned. Only one penetration depth (one-sixth through the wall) was considered
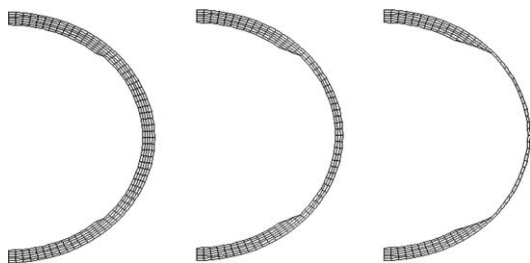
with the 'tenth' model (Case 2 of Table 5). The failure probability was found to increase suddenly with the initiation of the thinning process (Fig. 5). This occurs because thinning causes the SiC to detach from the IPyC, imposing stress concentrations in the SiC layer at the edges of the detached region. Thus, the probability increases significantly though the penetration depth is still essentially zero when the SiC first detaches from the IPyC in the thinned region. As shown in Fig. 5, though, the failure probability for these smooth transition models is not a strong function of penetration depth once thinning has been initiated. The failure probability for these models would, of course, jump to a value of 1.0 with full penetration through the SiC thickness (the thinned region extends around the circumference of the particle). Results also indicate that the failure probability is not strongly a function of the size of the thinned region. There is a relatively modest increase in going from the 'tenth' to the 'quarter' model, and only a small difference between the 'quarter' and 'half' models.

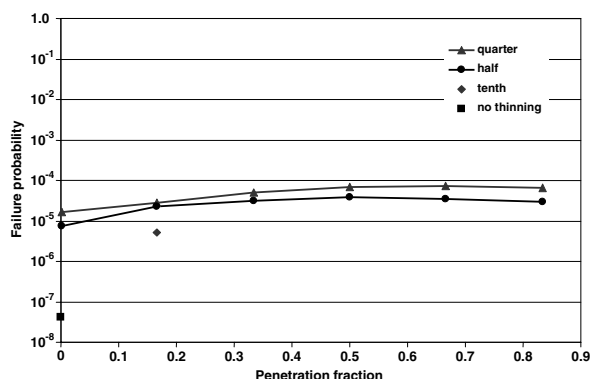Fig. 4. Axisymmetric model for SiC thinned over one-half its surface area.

Fig. 5. Failure probabilities for global models with smooth transition between thinned and nonthinned regions. (Penetrations were modeled to nodal locations at 0, 1/6, 1/3, 1/2, 2/3, and 5/6 of the SiC wall thickness.)

For both the sharp corner models of Table 5 and the smooth transition cases of Fig. 5, the failures evaluated were caused by shrinkage of the pyrocarbon layers, which induced stress concentrations at the edges of the thinned regions. The method used for determining particle failure probabilities for this behavior will follow what is currently used in PAR-FUME for other multi-dimensional failure mechanisms. In this approach, finite element analyses are performed on selected particles representative of the thinning scenario under consideration. The stresses calculated in these analyses capture the multi-dimensional behavior associated with SiC thinning. The particles selected for analysis also capture the effects of statistical variations in important input parameters. The same cases are analyzed with the one-dimensional stress solution in PAR-FUME to calculate stresses in corresponding nonthinned particles. Simple statistical fits are performed on the results of the analyses and correlations are drawn between stresses in multi-dimensional and one-dimensional particles for the same parametric variations. These correlations enable sampling over a large number of particles to determine a failure probability.

5. Thinning over a large portion of the SiC surface

5.1. Failures caused by shrinkage of the pyrocarbon layers

A three-dimensional model was developed to evaluate the effect of thinning over a large portion of the surface in a hemisphere of the SiC layer. In this model (Fig. 6), thinning was assumed to occur
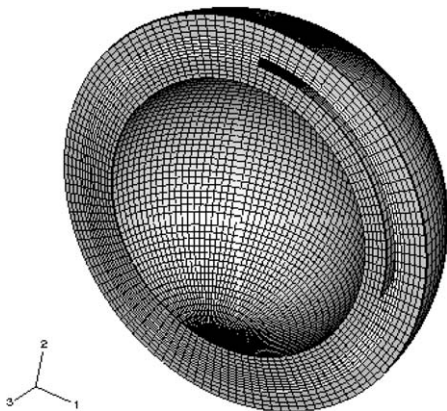

Fig. 6. Three-dimensional model for thinning over one-half a hemisphere of the SiC layer (one-quarter of full surface area).
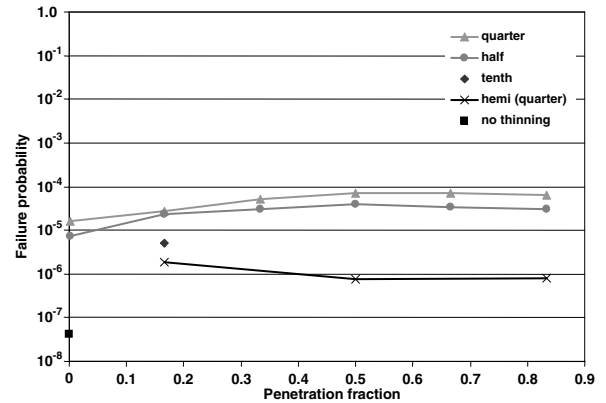

Fig. 7. Results from the three-dimensional model, thinning over one-half of a hemisphere in the SiC layer (dark curve). (Penetrations were modeled to nodal locations at 1/6, 1/2, and 5/6 of the SiC wall thickness.)

over one-half a hemisphere of the SiC layer (one-quarter of the total surface area). Models were developed for three penetration depths, i.e., one-sixth, one-half, and five-sixths of the SiC wall thickness. Failures considered with this model were those due to stresses induced by shrinkage of the pyrocarbon layers. Results are presented in Fig. 7, where they are compared to those from the previous global models. The failure probability for the hemispherical model [labeled 'hemi (quarter)'] is lower than for the previous models. This is because the highest stresses in this model were concentrated at the corners where the edges of the thinned region meet. In contrast, the maximum stresses in the axisymmetric models (at the edges of the thinned region) occur over the full circumference of the particle, and, therefore, occupy a larger fraction of the SiC volume. In the curve shown in Fig. 7, the failure probability is shown to be lower for a penetration fraction of one-half than for a penetration fraction of one-sixth. This occurred because the model in each case had the specified penetration depth from the start of the analysis. The failure probability for each point on the curve represents a situation where that depth of penetration had existed from the beginning of irradiation. In reality, the cumulative failure probability must either hold level or increase as the thinning process progresses. Since an actual particle would have to pass through low penetration fractions to reach higher penetration fractions, the failure probability used in actual failure evaluations will be the maximum occurring on the curve up to the penetration fraction attained.
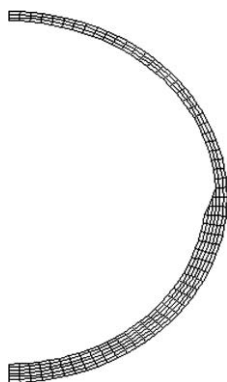
Fig. 8. Axisymmetric model for thinning over a hemisphere of the SiC layer to a depth of one-half thickness.

An axisymmetric model (Fig. 8) was suitable for analyzing the situation where thinning occurs over a full hemisphere of the SiC layer. Analyses were performed over a full range of penetration depths. As shown in Fig. 9, the results from this case (labeled 'hemisphere') are very similar to the previous case where thinning occurred over one-half of the SiC surface area (labeled 'half').

5.2. Failures caused by internal pressure loading

When thinning is assumed to occur over the full surface of the SiC layer, then the IPyC becomes fully detached from the SiC layer at the interface. If the IPyC layer successfully retains the internal pressure on its own, then the failure probability for the SiC is negligibly small. The thinning in this case makes essentially no contribution to particle failures. However, if the IPyC layer is breached due to the internal pressure, then the pressure load is fully transmitted to the SiC layer. The stresses for this situation were analyzed with an axisymmetric finite element model of a two-layer particle. They could as well be calculated with PARFUME's stress solution for a symmetrical two-layer particle. Results for two cases are presented in Fig. 10, where thinning is assumed to occur from the inside surface out [labeled 'full (in-to-out)'], and from the outer surface in [labeled 'full (out-to-in)']. The inside-to-out model represents thinning caused by fission product attack such as from CO reactions with the SiC, while the outside-to-in model represents thinning caused by an air ingress event or by thermal decomposition under certain conditions. Failure in either full model is caused by tangential stresses due to internal pressure. In both cases, a greater penetration due to thinning increases the SiC tangential stress, which in turn increases the failure probability. The sudden increase in failure probability at a zero penetration depth is a result of the transition from a three-layer to a two-layer particle as either the IPyC or OPyC detaches from the SiC.

In the analyses of the outside-to-in model, the OPyC layer was assumed to detach from the SiC, and was removed from the model at the outset of the analysis. The results of Fig. 10 are based on this assumption. In actual performance model evaluations, the OPyC will not necessarily be detached immediately from the SiC at the initiation of SiC thinning. If the OPyC is present, it will still shrink inward and maintain contact with the SiC until
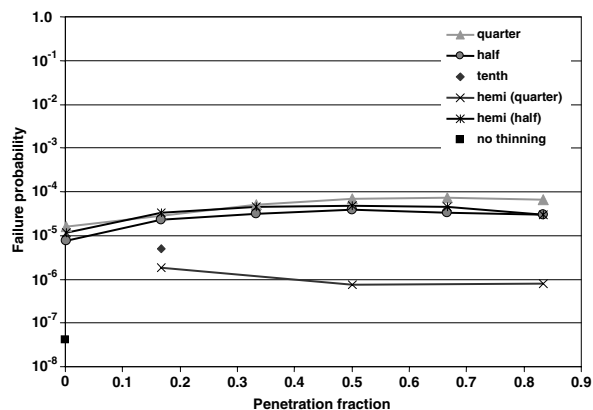

Fig. 9. Results for thinning over a full hemisphere of the SiC, compared with other results. (Penetrations were modeled to nodal locations at 0, 1/6, 1/3, 1/2, 2/3, and 5/6 of the SiC wall thickness.)
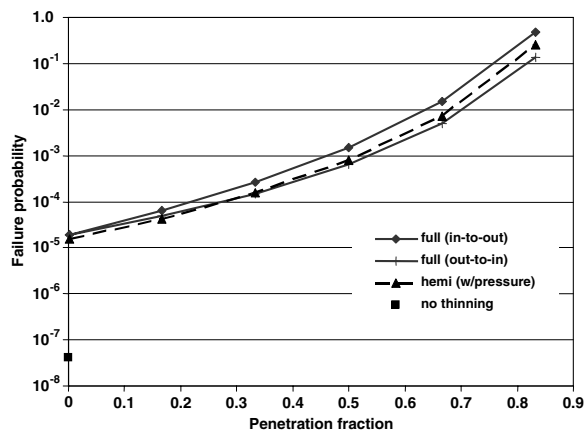

Fig. 10. Results for thinning over the full (or half) surface of the SiC, internal pressure directly transmitted to the thinned region. (Penetrations were modeled to nodal locations at 0, 1/6, 1/3, 1/2, 2/3, and 5/6 of the SiC wall thickness.)

the thinning effect outweighs the shrinkage effect. This will delay the initial increase in failure probability shown in Fig. 10 for the 'full (out-to-in)s' case until detachment occurs.

In any situation where thinning occurs over a significant portion of the SiC inner surface area, the associated detachment of the IPyC from the SiC over that region could significantly increase the probability that the IPyC would fail. Failure of the IPyC is caused in this case by the significant increase in IPyC tangential stress (due to gas pressure) once contact is lost between the IPyC and SiC. Since contact is lost in the corroded region of the SiC, it is expected that failure of the IPyC will occur in that location. Because the IPyC crack is located in the corroded area, it allows the pressure to be directly transmitted to the SiC in that area. The likelihood of particle failure increases when just the SiC and OPyC layers resist the pressure and the SiC thickness is reduced. Shown in Fig. 10 are the results for a case [labeled 'hemi (w/pressure)'] where thinning occurred over a hemisphere of the SiC, and the internal pressure was applied directly to the SiC over the thinned region. The internal pressure induces membrane and bending stresses in the SiC layer, resulting in a failure probability that is of the same order of magnitude as that of a particle that is thinned over the full surface.

Based on these results, the criterion used in PARFUME for the failure of thinned particles due to internal pressure loading will include an evaluation for failure of the IPyC layer. If the IPyC fails, the potential for subsequent failure of the SiC due to internal pressure loading will also be evaluated. When the full internal pressure load is applied to the entire IPyC or SiC surface area, these evaluations will follow traditional methods for analyzing pressure vessel failure in one-dimensional (symmetrical) particles. When the pressure is applied to only a portion of the IPyC or SiC surface area, then stresses in these layers can be estimated using analytical methods for pressure loading applied to a partial spherical shell [9], or can be determined with finite element analysis. An advantage of the analytical method is that it can be programmed into the performance code. An analytical approach for determining stresses in the SiC, though, becomes complicated because of the attached OPyC layer. Based on results shown in Fig. 10, the failure probability for pressure loading on a partial sphere is expected to be within an order of magnitude of the probability for a full sphere. Analyses on

enough of these cases may show that an adjustment to the probability for a full sphere can be made to estimate the probability for a partial sphere based on the size of the thinned area, without having to perform multi-dimensional stress analyses.

Finally, Fig. 11 presents a compilation of results from all analyses performed involving global
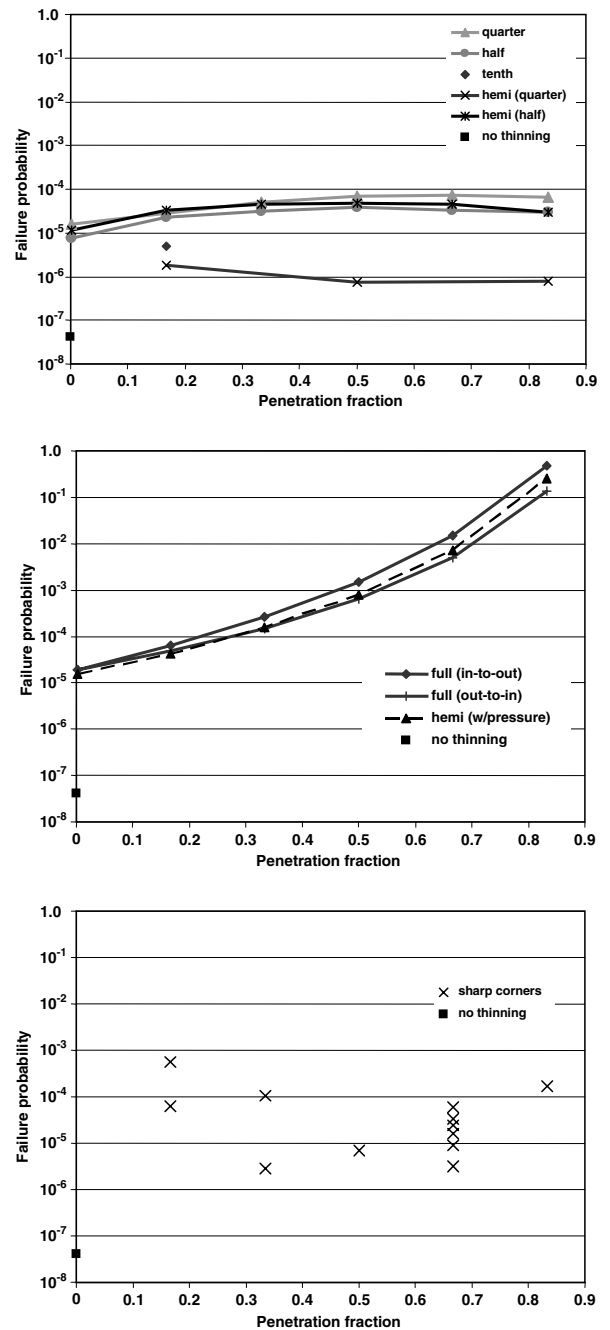

Fig. 11. Compilation of results for all cases analyzed.

thinning, including the sharp corner cases from Table 5. Because the failure probability for cases involving sharp corners is sensitive to the depth and width of the thinned region, results for those cases show a degree of scatter.

6. Conclusions

Numerous analyses have been performed to evaluate the effects of thinning of the SiC layer on the failure probability for TRISO-coated particles. Results of these analyses are intended for use in developing an approach for incorporating this failure mechanism in a fuel performance code. The factors evaluated were local and global thinning, size of the thinned region (width and depth), the number of locations at which thinning occurs, sharp corners and smooth transitions at the edges of the thinned regions, and stresses caused by shrinkage of the pyrocarbon layers and by internal pressure loading.

Results showed that thinning of the SiC in local areas (e.g., by palladium or fission product nodule attack) makes a negligible contribution to the particle failure probability when considering failures of the SiC due to stresses in the layer. However, complete penetration through the SiC provides an open path for fission product transport, and, therefore, constitutes a functional failure of the particle. Thus, the recommended failure criterion for local thinning is that failure occurs when penetration through the full thickness is achieved.
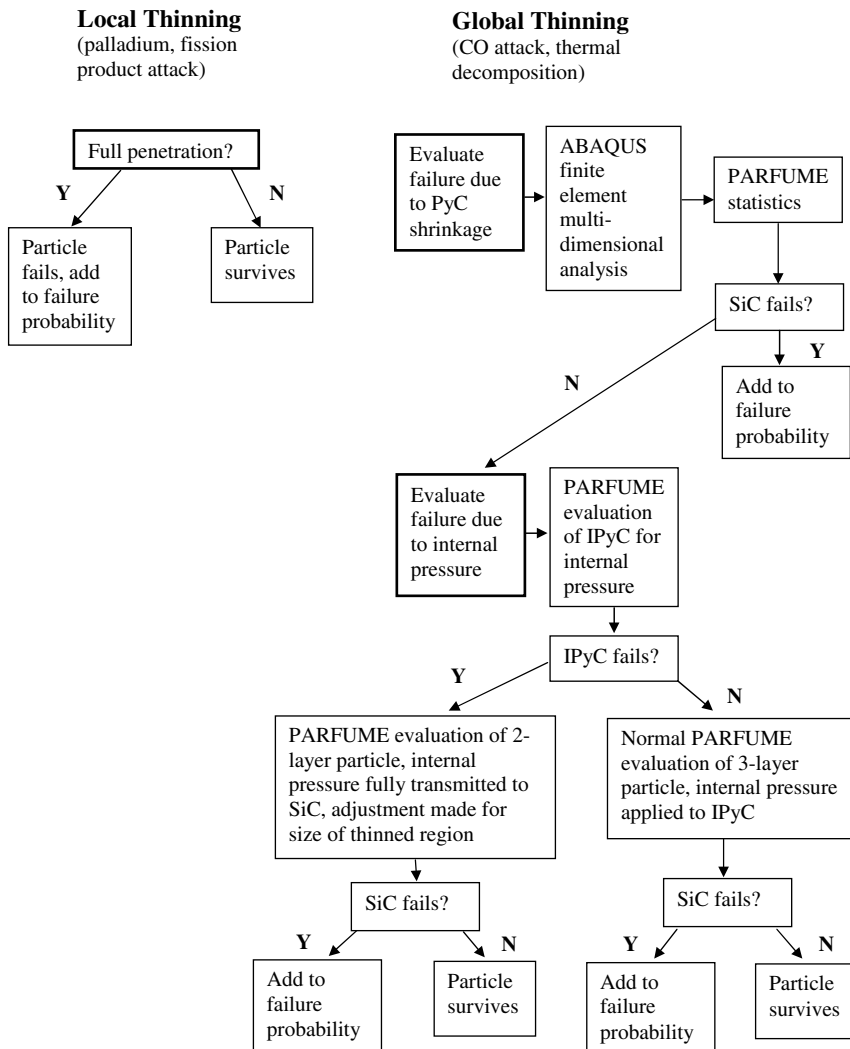

Fig. 12. Flowchart showing logic for evaluating particle failures due to SiC thinning.

For thinning over global areas of the SiC (extending around the circumference of a particle or over a large portion of the SiC surface area), failures can occur due to stress concentrations at the edges of the thinned regions induced by shrinkage of the pyrocarbons. The resulting failure probability is sensitive to the width and depth of the thinned region and also to the number of thinned locations when sharp corners exist at the transition between the thinned and nonthinned regions (which is probably typical of thinning over narrow regions). When the transition at the edges of the thinned region is smooth, however, the failure probability is relatively insensitive to the depth of penetration and only moderately sensitive to the size of the thinned area. The method for determining particle failure probabilities for these situations follows what is currently used in PARFUME for other multi-dimensional failure mechanisms. Finite element analyses are performed on selected particles representing the thinning scenario under consideration. These analyses capture the multi-dimensional behavior and the effects of statistical variations in important input parameters. Results of these analyses are then imported into PARFUME, where statistical correlations are employed to determine a failure probability.

When the SiC is thinned over a significant portion or all of its surface area (e.g., CO attack or thermal decomposition), the detachment of the IPyC from the SiC over this portion of the interface between layers enhances the probability that the IPyC will fail due to internal pressure loading. If the IPyC fails, then the internal pressure loading is directly transmitted to a portion or all of the SiC surface area, which can lead to failure of the SiC layer. If the IPyC alone cannot sustain the internal pressure in the thinned area, then the failure probability of the SiC layer can be substantially increased, especially as the penetration depth increases. Thus, the criterion used in PARFUME for the failure of thinned particles due to internal pressure loading will include an evaluation for failure of the IPyC layer. If the IPyC fails, then potential for subsequent failure of the SiC will be evaluated. If the full internal pressure acts on the entire IPyC or SiC surface, then failure of these layers can be evaluated

using traditional methods for one-dimensional (symmetrical) pressure vessels. If the full pressure acts on only a portion of the IPyC or SiC surface, then stresses in the evaluation are based on loading of partial spherical shells. The failure probability for a sphere that is thinned over a part of its surface is expected to be within an order of magnitude of the probability for a sphere thinned over its entire surface. Therefore, it may be possible to estimate its failure probability by simply making an adjustment to the probability for a full (symmetrical) sphere based on the size of the thinned surface area.

The accuracy of calculated failure probabilities is sensitive to uncertainties in the material properties, such as the Weibull characteristic strength and modulus for the SiC layer. Acquiring reliable data for the material properties should improve the accuracy of the probability calculations. Also, a crack propagation model based on fracture properties of the corroded SiC could show the SiC material to be more vulnerable to failure than realized in these analyses.

Fig. 12 presents a flowchart showing the recommended logic for incorporating SiC thinning into the fuel performance code.

References

[1] G.K. Miller, D.A. Petti, D.J. Varacalle, J.T. Maki, J. Nucl. Mater. 295 (2001) 205.
[2] G.K. Miller, D.A. Petti, J.T. Maki, J. Nucl. Mater. 334 (2004) 79.
[3] NP-MHTGR Material Models of Pyrocarbon and Pyrolytic Silicon Carbide, CEGA Corporation, CEGA-002820, Rev. 1 July 1993.
[4] J. Kaae, D. Stevens, C. Luby, Nucl. Technol. 10 (1971) 44.
[5] D.G. Martin, Physical and mechanical properties of constituents of coated fuel particles and the effect of irradiation, HTR-F WP3 Meeting, Lyon, 2001.
[6] G.K. Miller, D.A. Petti, D.J. Varacalle, J.T. Maki, J. Nucl. Mater. 317 (2003) 69.
[7] ABAQUS Analysis User's Manual, Version 6.4, 2003.
[8] N.N. Nemeth, J.M. Mandershield, J.P. Gyekenyesi, Ceramics Analysis and Reliability Evaluation of Structures (CARES) User's and Programmer's Manual, NASA Technical Paper 2916, 1989.
[9] S. Timoshenko, S. Woinowsky-Krieger, Theory of Plates and Shells, McGraw-Hill Book Company, New York, 1959, p. 533.